Renewable and Sustainable Energy Reviews 13 (2009) 2012–2021

Contents lists available at ScienceDirect

Renewable and Sustainable Energy Reviews

journal homepage: www.elsevier.com/locate/rser

Reliability and cost analyses of electricity collection systems of a marine current farm—A Taiwanese case study

M.Q. Lee [a], C.N. Lu [a], H.S. Huang [b,*]

[a] Department of Electrical Engineering, National Sun Yat-Sen University, No. 70, Lienhai Rd., Kaohsiung 804, Taiwan, ROC
[b] Department of Electrical Engineering, Ching Yun University, No. 229, Chien-Hsin Rd., Jung-Li 320, Taiwan, ROC

ARTICLE INFO

Article history:
Received 24 October 2008
Accepted 21 January 2009

Keywords:
Reliability analysis
Cost analysis
Electricity collection systems
Marine current farm
Taiwan

ABSTRACT

The exploration of ocean energy for electric power production offers a sustainable option to enhance the use of renewable energy. In this article, the reliability and cost analyses results of electricity collection systems proposed for a marine current farm are presented. A methodology based on the probability density function of site current speed is developed to determine the speed specifications of marine current turbine. Reliability analyses are conducted by taking electricity collection structure, equipment failure rate and probability distribution of turbine power output into account. Non-delivered energy cost in conjunction with the investment cost, power loss, operations and maintenance costs are included in the cost analyses. Ocean current speed data measured at the Taiwan coastline situated in the Kuroshio stream path are used to calculate the life-cycle costs of the studied energy collection systems. Simulation results show that marine turbine parameters can be effectively specified, and a sectionalized radial collection structure provides an efficient scheme for harnessing ocean energy.

Contents

1. Introduction

While large offshore wind farms are becoming popular, in large areas with high currents, it will be possible to install marine turbines in groups or clusters to make up a marine current farm. The basic physics of a marine current turbine (MCT) are similar to

* Corresponding author. Tel.: +886 3 4581196x5320; fax: +886 3 4594937.
E-mail address: hshuang@cyu.edu.tw (H.S. Huang).

1364-0321/$ – see front matter © 2009 Elsevier Ltd. All rights reserved.
doi:10.1016/j.rser.2009.01.011

Nomenclature

A	swept area of the marine current turbine (m^2)
C_I	initial investment cost ($)
C_p	power coefficient
C_{PF}	present value cost of the fixed loss cost ($)
C_{PNDE}	present value cost of the non-delivered energy cost ($)
C_{POM}	present value cost of the operation and maintenance cost ($)
C_{PV}	present value cost of the variable loss cost ($)
CF	capacity factor
D_n^α	a critical value in standard table calculated based on sample size n and significance level α
$f(v)$	current speed probability density function
FC	future cost being paid for each year ($/year)
$irate$	discount rate
LCC	life-cycle cost ($)
nlc	life-cycle period of equipment (year)
N_s	number of operating states
NDE	non-delivered energy (MWh/year)
P_e	electrical power output (MW)
$P_{e,avg}$	average electrical power output (MW)
$P_{e,i}$	average power output of marine current turbine i (MW)
$P_{e,R}$	rated electrical power output (MW)
P_N	normalized average power
$P(x)$	cumulative normal distribution function
$Prob_s$	probability of a turbine availability state (or a generation state)
PW	present worth ($)
Q	forced outage rate of a marine current turbine
$S_n(x)$	the sample cumulative distribution with sample size n
TPI	turbine performance index
U_i	unavailability of marine current turbine i
V_C	cut-in speed of marine current turbine (m/s)
V_F	cut-out speed of marine current turbine (m/s)
V_R	rated speed of marine current turbine (m/s)

Greek symbols

β	standard deviation bounds
η	efficiency of drive train
μ	mean value of the normal distribution function (m/s)
ρ	sea water density, which is about 1024 (kg/m^3)
σ	standard deviation of the normal distribution function (m/s)

those of a wind turbine. The power available is proportional to the working fluid density and cubic of its speed. MCTs have lower rotational speeds than wind turbines, but since the density of sea water is much higher, the power output from an MCT is higher than that from a wind turbine of equivalent blade size, or alternatively, MCTs can be much smaller than wind turbines to generate as much power. MCT technologies are being developed in many countries [1]. Small-scale systems were deployed and tested. For a large-scale system which covers a wider area, for economic reasons, the current speed characteristics, reliability and cost of electricity collection system have to be investigated.

The power output of an MCT depends upon the mean and distribution of current speeds at the site, and the operation characteristics of the MCT. The choice of cut-in, cut-out and rated speeds of MCT should match the current conditions in order to bring its potential into full play. In the wind farm development, it has been shown that wind speed at a location can be statistically modeled by a Weibull probability density function. In [2], Jangamshetti and Rau presented a method of matching wind turbine generators to site wind speed characteristics. This technique identifies optimum turbine speeds from a turbine performance index (*TPI*) curve that is obtained from the normalized power and capacity factor curves.

Establishing a marine current farm requires a large investment and it is crucial to maximize the power output in order to shorten the pay back time. Using the Kolmogorov–Smirnov test technique and investigating a few different distributions, it is concluded that normal distribution is more adequate for describing the ocean current speed recorded in this study. This difference in speed distribution is essential and should be paid attention if techniques adopted in wind turbine design are to be used in the MCT design.

Bahaj and Myers proposed a method to assess the potential of electricity generation at Alderney Race in the Channel Islands [3]. This work quantified the resource and identified currents that could be used for the establishment of various size arrays in the Race. Predicted resource was 7.4 TWh which is equivalent to 2% of UK requirements in the year 2000. However, in that work unavailability and power loss of electricity collection scheme were not considered.

Reliability is critical, since accessibility to the offshore marine current farm may be limited during certain times of the year due to adverse weather conditions. Experiences from the Middelgrunden offshore wind farm reported in [4] showed that, while the availability of the wind turbines was around 98%, the availability of the whole wind farm including the 30-kV collection grid was at least 2% lower.

Sannino et al. analyzed the availability of three different collection schemes within a wind farm [5]. The energy not produced due to outages in the wind farms was calculated and sensitivity of the results to variations in failure rate and mean time to repair of cables and apparatus was presented. In [6], a comparative analysis of various design options for electricity collection system of large offshore wind farms was presented. The advantages and disadvantages in terms of their steady-state performance, such as power losses, voltage level changes, contingency analysis, and economics were discussed. Four basic designs of energy collection systems: radical design, single-sided ring design, double-sided ring design and star design were analyzed. According to the steady-state test results, a single-sided ring arrangement is a better option for a large offshore collector system as it achieves fewer losses in both, normal and contingency operations. However, the results of the economic assessment have shown that the cost of the associated redundant circuit required by this design is very likely to become an economic barrier, particularly when compared with the cheaper option of a typical radical design. In that study, the economic assessment was based only on the investment cost and system power loss. Unavailability costs were not considered.

In this article, the reliability and cost analyses of various electricity collection schemes for an offshore marine current farm are presented. In the analyses, the MCT speed parameters are chosen to match the characteristics of offshore current at northeast coast of Taiwan. *TPI* formulation used to determine suitable turbine parameters for better asset utilization is derived. With the calculated MCT average power output, life-cycle cost (*LCC*) of five different electric power collection schemes are presented. The procedure and methodologies involved in the analyses are shown in Fig. 1. Details are given in the following sections.

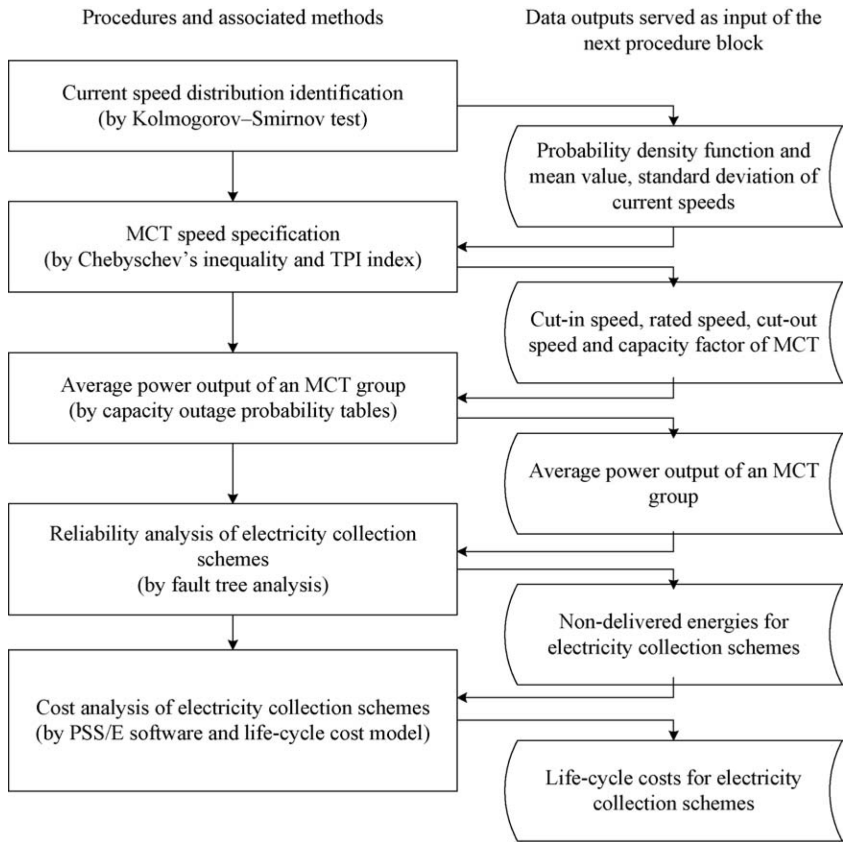


Fig. 1. The procedure used for reliability and cost analyses of marine current farm electricity collection systems.

2. Matching turbine specifications with current characteristics

2.1. Identification of ocean current speed distribution

The first step in assessing the energy potential of a proposed marine current farm is to identify its current speed distribution. The hourly ocean current speed data recorded at the Su-ao anchor station are used in this study. Fig. 2 shows a sample distribution of occurring frequencies of the current speeds at 30 m below sea level. Higher current speed locations are being searched. In the following presentation the data shown in Fig. 2 are used.

Kolmogorov–Smirnov test (K–S test), which quantifies a distance between the empirical cumulative distribution function of the sample and the cumulative distribution function of a hypothesized distribution, is a goodness-of-fit test and appropriate for testing sample data against a continuous distribution [7]. In this test, if the value of the maximum deviation exceeds the critical value, one rejects the hypothesis that the sample is from the hypothesized distribution. It is used in this study and distributions such as normal, Weibull, Rayleigh and other distributions were tested.

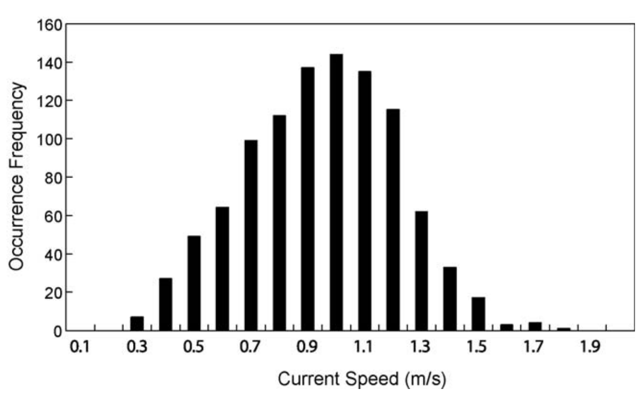


Fig. 2. Current speed distribution of Su-ao station.

If the hypothesized distribution is a normal distribution, the procedure of K–S test is as follows. Given a sample of n speed observations, one determines $D = max_x|P(x) - S_n(x)|$, where $S_n(x)$ is the sample cumulative distribution and $P(x)$ is the cumulative normal distribution function with $\mu = \bar{X}$, the sample mean, and $\sigma^2 = s^2$, the sample variance. If D is less than D_n^{α}, which is a critical value in standard table calculated based on sample size n and significance level α, then the sample data follow the normal distribution. If $D > D_n^{\alpha}$, one rejects the hypothesis.

For the 1009 data shown in Fig. 2, if the significance level is 0.05, then $D_n^{\alpha} = D_{1009}^{0.05} = 0.0428$. $D = max_x|P(x) - S_n(x)| = 0.0252$, which is less than D_n^{α}. Test results indicate that normal distribution is suitable for describing the characteristics of the current speeds measured at different depth of the studied site.

2.2. MCT speed specification

MCT power output depends upon the mean current speed, cut-in, cut-out and rated speeds of MCT. Thus, there is a need for developing a method to identify optimal speed parameters of MCTs in order to deliver higher average power at higher capacity factor. Table 1 shows some of the current MCT technologies [8].

The MCT outputs can be represented by their V–P (current velocity–power output) curves as shown in Fig. 3. Fig. 3(a) shows a model that the rated speed is the same as cut-out speed. Models MCT-A to MCT-G shown in Table 1 have such V–P curves. MCT-H is a model that uses rotor pitch-control and has a flat rated output region between the rated speed and cut-out speed as shown in Fig. 3(b). V–P curve shown in Fig. 3(b) is used in this study and the

Table 1
Parameters of some marine current generators [8].

Types	Cut-in speed (m/s)	Rated speed (m/s)	Cut-out speed (m/s)	Rating (kW)
A	0.5	2.58	2.58	6.95
B	1	3.1	3.1	2000
C	0.7	2.57	2.57	1520
D	0.7	3	3	44
E	0.7	2.3	2.3	1000
F	1.54	3	3	400
G	0.7	2.2	2.2	38
H	0.7	3.1	3.5	2548

power output can be expressed as:

$$P_e(v) = \begin{cases} 0 & \text{for } v < v_C \text{ or } v > v_F \\ \frac{1}{2}\rho A C_p \eta v^3 & \text{for } v_C \le v \le v_R \\ \frac{1}{2}\rho A C_p \eta v_R^3 & \text{for } v_R < v \le v_F \end{cases} \quad (1)$$

where ρ is the sea water density, A is the swept area of the MCT, C_p is the power coefficient, η is the efficiency of drive train, v_C is the cut-in speed of MCT, v_R is the rated speed and v_F is the cut-out speed.

TPI that takes both capacity factor (*CF*) and power output into account is utilized in this study to specify MCT speed parameters. It is defined as

$$TPI = \frac{P_N \times CF}{P_{N,max} \times CF_{max}} \quad (2)$$

where P_N is the normalized average power. *CF* indicates average usage of the assets, is equal to the average output power divided by turbine's rated output power. It can be derived based on the speed distributions determined. If cut-in, cut-out and rated speeds are chosen as independent variables, and $f(v)$ is the current speed probability density function, *CF* is expressed as

$$\begin{aligned} CF &= \frac{P_{e,ave}}{P_{eR}} = \frac{\int_0^\infty P_e(v) f(v)\,dv}{P_{eR}} \\ &= \frac{\int_{v_C}^{v_R} (1/2)\rho A C_p \eta v^3 f(v)\,dv + \int_{v_R}^{v_F} (1/2)\rho A C_p \eta v_R^3 f(v)\,dv}{(1/2)\rho A C_p \eta v_R^3} \\ &= \frac{1}{v_R^3}\int_{v_C}^{v_R} v^3 f(v)\,dv + \int_{v_R}^{v_F} f(v)\,dv \end{aligned} \quad (3)$$

Details of the *CF* derivation are shown in Appendix A. A normalized average power obtainable from MCT is defined as [2]

$$P_N = \frac{P_{e,ave}}{(1/2)\rho A C_p \eta} = \frac{P_{eR} \times CF}{(1/2)\rho A C_p \eta} = v_R^3 \times CF \quad (4)$$

The speed specifications of marine turbine will affect *CF* and they should be determined based on the actual current speed characteristics. If a higher *CF* is desired, then turbine rated speed cannot be chosen too high such that the system can operate at rated power output condition for most of the time, but in this case, much of energy in higher speed currents would not be harvested. On the other hand, if the *CF* is chosen too low, then although the system can yield a higher amount of output at rated speed, the turbine would seldom operate at its rated capacity and lose much of the energy of lower speed current.

From the current MCT technologies shown in Table 1, one could choose an MCT with the highest *TPI* value or to maximize the *TPI* by specifying the speed parameters of the MCT. In this study, the rated speed v_R is chosen to maximize *TPI* with the pre-specified v_C and v_F, that are determined based on site current speed distribution and the Chebyschev's inequality [9] shown in the following.

$$f(|v - \mu| \ge \beta\sigma) \le \frac{1}{\beta^2} \quad (5)$$

where μ is the mean value of the normal distribution function of current speed, σ is the standard deviation and β is the standard deviation bounds.

Since the mean value and standard deviation of a normal distribution are sufficient to make statements on the probability of speeds within given upper and lower boundaries, these bounds can be used to specify v_C and v_F.

2.3. Average power output of an MCT group

The wake of upstream turbines may interfere with downstream turbines, reducing the amount of energy produced. In a wind farm, the wake effect is a function of wind turbines spacing (both downwind and crosswind), wind turbine operating characteristics, the number of turbines, size of the wind farm, turbulence intensity and frequency distribution of the current direction [10]. In a marine current farm, distance between MCTs may be large in order to avoid wake effect. To simplify the reliability model of a large marine current farm, the wake effect is neglected and a group of MCTs in a neighboring area are aggregated. The average power output of the group is calculated by using the capacity outage probability table [11]. As the name suggests, it is a simple array of capacity levels and the associated probabilities of existence. For a group of m MCTs, each has a forced outage rate of Q, the probability of a turbine availability state (or a generation state), $Prob_s$, with s machines up and m–s machines down, can be calculated by the following equation:

$$Prob_s = \prod_{i=1}^{s}(1 - Q)\prod_{j=s+1}^{m} Q \quad (6)$$

The average power output of the MCT group is the summation of multiplications of state probability and amount of power output in that state. Repair time and forced outage rate could be high due to offshore environment and affect the average power output.

3. Reliability and cost analyses of electricity collection schemes

3.1. Electricity collection schemes

MCT equipments are interconnected in strings by sub-sea cables. The strings are then connected to the platform by feeder

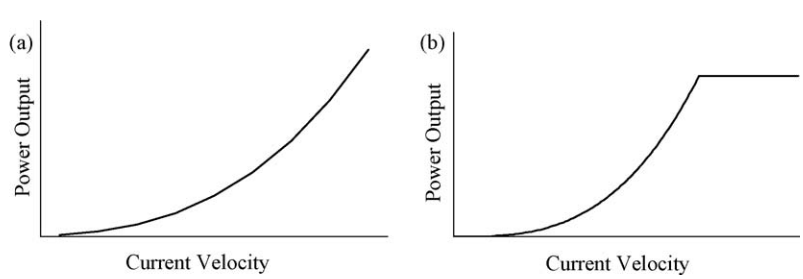


Fig. 3. *V–P* curves of MCTs.

cables. The cables together with necessary switching equipment, such as fuse, breakers, dis-connectors, etc., form the collection grid. There are various possible arrangements for the energy collection. Based on schemes suggested for offshore wind farms [5,6], the authors identified five basic electricity collection designs for the studied marine current farm.

Radial design (scheme a) is the most straightforward arrangement. Fig. 4(a) shows a radial design with circuit breakers at platform. In this case, the MCT equipment shown aggregates five 1 MW MCTs. The maximum number of MCT equipments on each string feeder is determined by the capacity of the generators and the maximum rating of the sub-sea cable. This design offers the benefits of being simple and inexpensive because the total cable length is smaller. The major drawback of this design is its poor reliability as cable or switchgear faults at the platform end of a radial string would prevent all downstream turbines from exporting power.

Fig. 4(b) illustrates a ring design (scheme b), where two strings are interconnected in a ring system with a few sectionalizing breakers and the ring is connected to the platform by one breaker. If the full output power of the MCT equipments in one of the strings were to be transferred through the other string during special situations, then the cable needs to be sized to a higher rating.

U-ring design (scheme c) shown in Fig. 4(c) is similar to the ring design. Each string of MCT equipments is connected to the platform with a feeder cable, and the other end of one string is connected to the next forming a ring (U-ring). The redundancy offered by the ringed designs is beneficial when the probability of a fault and the associated costs are higher than the costs associated with additional equipment, especially, when the repair downtimes are long. However, it should be pointed out that the fault current of a ring structure will be higher than that of a radial structure and could result in a higher requirement in switchgear rating.

The star design (scheme d) illustrated in Fig. 4(d) can be used to reduce cable ratings and provide a high level of security, since one cable outage only affects one MCT equipment. However, there is additional expense in longer diagonal cable runs and some short sections of higher rated cabling.

The fifth scheme will be presented later. In Fig. 4, a three-winding step-up transformer in the platform is also shown. This is the same for all topologies and is not included in the analysis presented.

3.2. Reliability assessment of electricity collection system

Reliability analyses can be conducted with relatively simple calculations by using the network reduction method [11], which creates a sequence of equivalent components obtained by gradually combining series and parallel components. Fault tree analysis is also a popular technique, in which a particular failure condition, known as the top event, is considered, and a tree is constructed by identifying various combinations and sequences of other failures that lead to the failure being considered. The process starts by first identifying a specific mode of system failure to be assessed. The causes of this operation mode are gradually broken down into an increasing number of hierarchical levels until a level is reached at which the

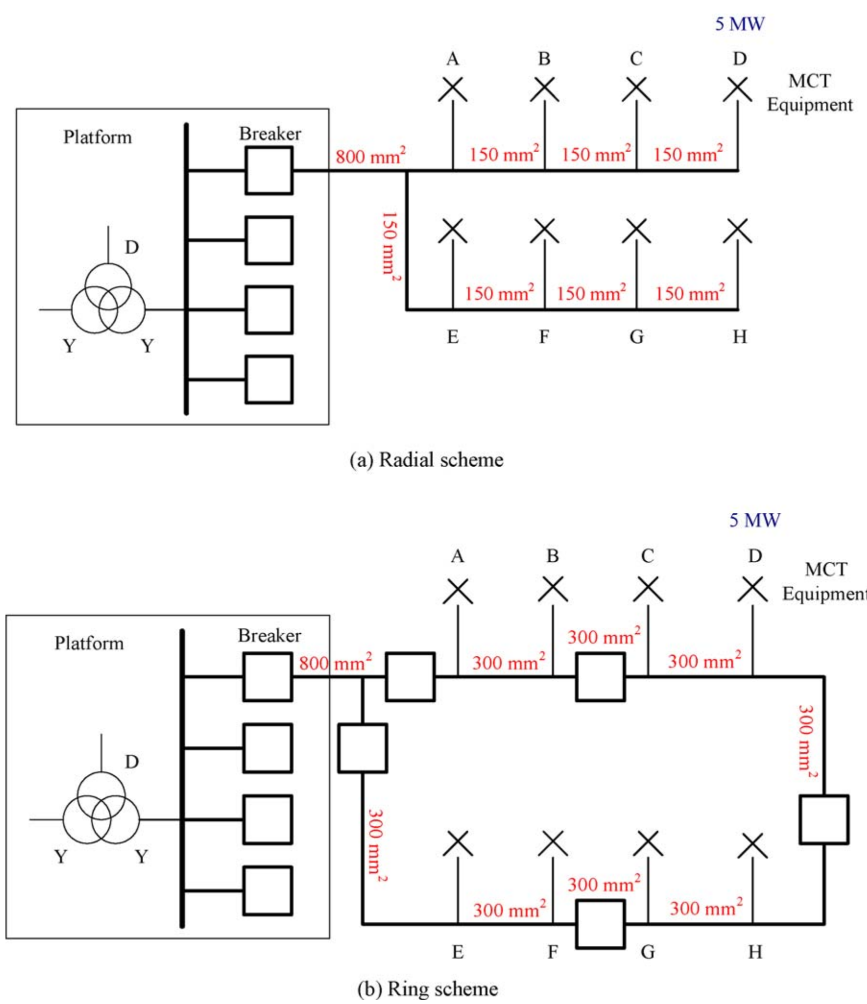
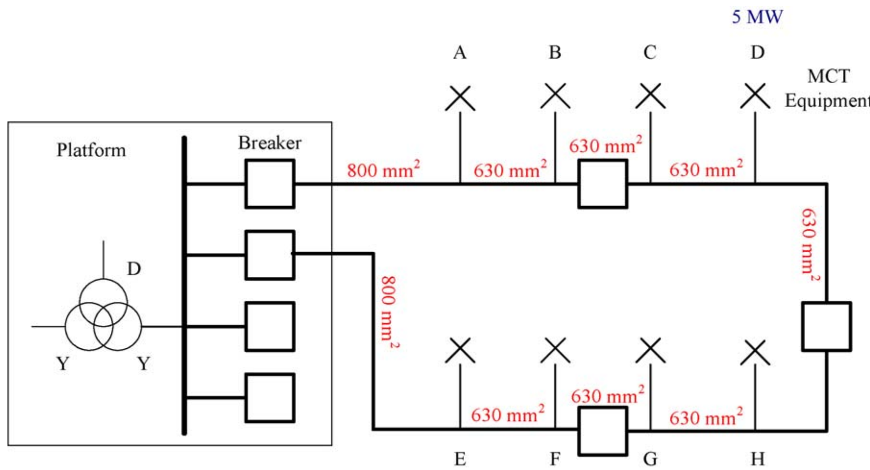
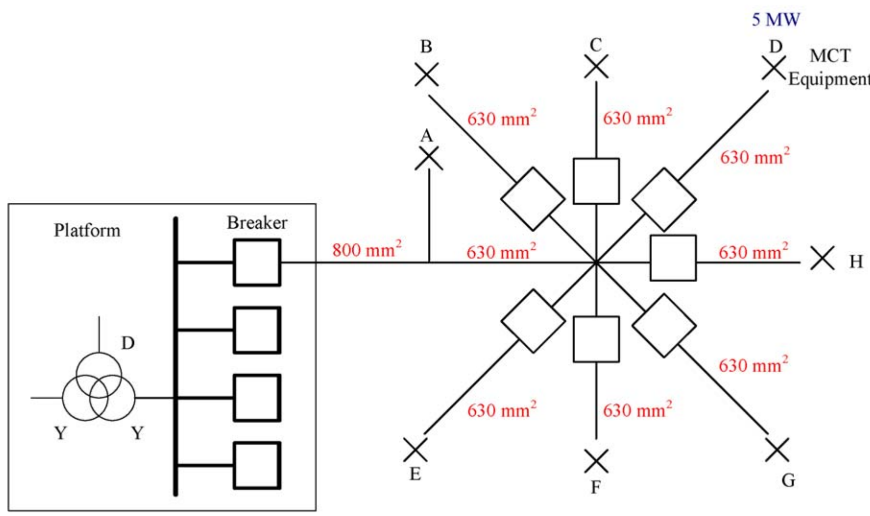


Fig. 4. Electricity collection schemes.



(c) U-ring scheme



(d) Star scheme

Fig. 4. (*Continued*).

behavior or effects of failure of the basic system components can be identified. The fault tree analysis is adopted in this work. Fig. 5 shows a fault tree that MCT-A cannot deliver power to the platform for scheme a. A complete model of each collection scheme can be built based on the interconnection structure of the scheme. Combining all the basic events together using the properties of Boolean algebra and the logical structure of the fault tree, the probability of the top event of a fault tree can be calculated.

Different reliability indices can be used for different purposes, such as expected generated marine energy, average service availability index, non-delivered energy (*NDE*), and average service unavailability index. In this study, the *NDE* index defined in the following is adopted.

$$NDE = \sum_{i=1}^{N_s} P_{e,i} U_i \tag{7}$$

where $P_{e,i}$ is the average power output of MCT i, U_i is its unavailability and N_s is the number of operating states.

3.3. Cost analyses

A specific design choice may have a complex effect on the project financial performance, affecting capital costs, taxes, insurance, energy revenue, maintenance costs, and government subsidies. In this study a simplified calculation based on minimizing *LCC* of ownership and operation of the network, is used to compare different design options. A scheme with minimum *LCC* that balances the capital investment against the costs of system operation and maintenance (O&M) and energy losses is preferred.

There are three unique types of energy losses, each affecting the revenue model in a different way, they are [12]:

(1) Fixed losses which do not vary with turbine output. These losses are primarily transformer excitation losses.
(2) Variable load losses which are ohmic losses in cables and transformers.
(3) Energy non-delivered due to a constraint imposed by electrical system unavailability.

Present values of the costs and losses in the system life time translate annual costs and lost energy production into an equivalent initial capital cost. The *LCC* of a studied system can be defined as

$$LCC = C_I + C_{POM} + C_{PF} + C_{PV} + C_{PNDE} \tag{8}$$

where C_I is the initial investment cost, C_{POM} is present value cost of the operation and maintenance cost, C_{PF} is present value cost of the

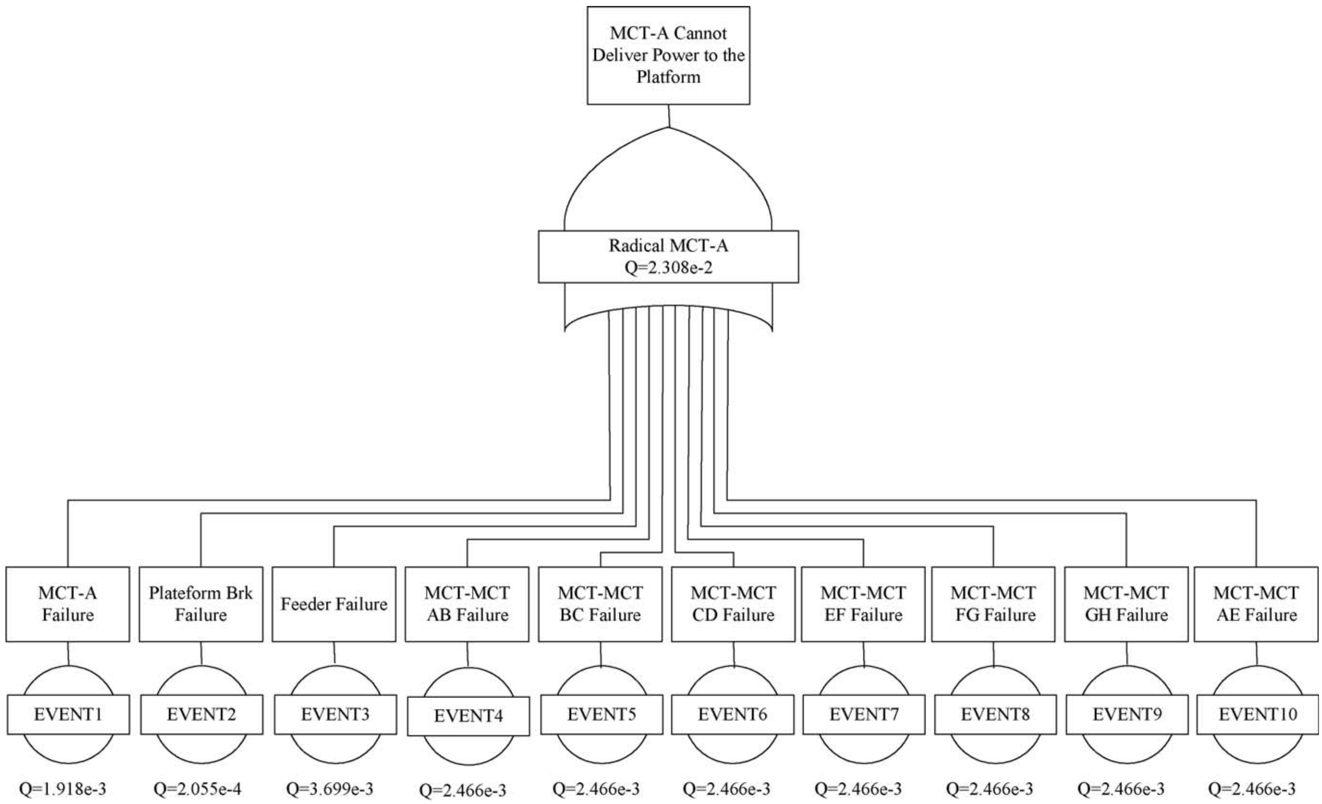


Fig. 5. A fault tree example for scheme a.

fixed loss cost, C_{PV} is present value cost of the variable loss cost and C_{PNDE} is present value cost of the *NDE* cost.

The cost transformation from future value to present value is based on following equation

$$PW = FC\left[\frac{(1 + irate)^{nlc} - 1}{irate \times (1 + irate)^{nlc}}\right] \tag{9}$$

where *PW* is the present worth, *irate* is the discount rate, *nlc* is the life-cycle period of equipment and *FC* is the future cost being paid for each year.

4. Analyses results and discussions

4.1. MCT speed specification results

Ocean current data shown in Fig. 2 are used for turbine speed parameter specification. As shown in Fig. 6, if the probability of the speed of ocean current exploited to generate electric power is chosen to be 0.8, then the probabilities outside the upper and lower bounds are 0.1 and 0.1, respectively, and from Chebyschev's inequality shown in (5), $1/(2\beta^2) = 0.1$, β is 2.236. The speeds corresponding to the lower and upper bounds are $\mu - \beta\sigma = 0.3015$ (m/s) and $\mu + \beta\sigma = 1.4910$ (m/s) respectively. These could be chosen as the cut-in and cut-out speeds of the turbine. However, after considering the current marine turbine technology (Table 1), the cut-in speed is set to 0.5 m/s.

With the specified v_C and v_F, the *CF*, P_N and *TPI* curves are calculated and shown in Fig. 7. It can be seen that P_N and *CF* curves reach their peaks at different rated speeds and implying that a compromise should be made to achieve the best result. Since *TPI* curve takes *CF* and normalized power factors into to account, its peak can be used to specify the rated speed of the turbine. The turbine specifications are summarized in Table 2.

4.2. Average power output of a MCT group

The MCT group shown in Fig. 8 has five 1 MW MCTs and each has a forced outage rate of 0.05, excluding the consideration of bus bar and transformer failures for simplicity, the probabilities

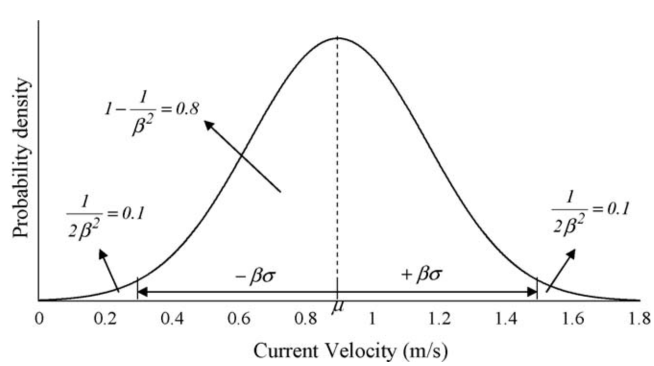


Fig. 6. Normal distribution representation of current speeds.

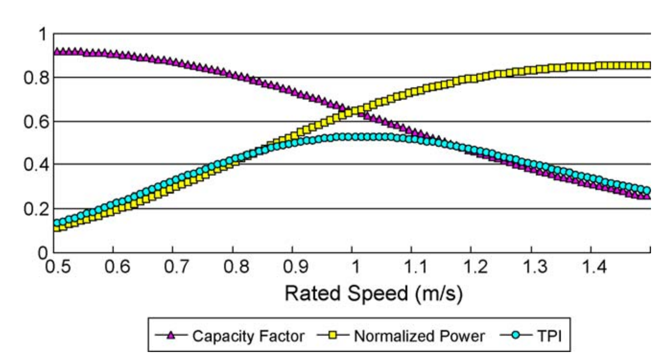


Fig. 7. The capacitor factor, normalized power, and *TPI* curves.

Table 2
MCT specifications.

Parameters and calculated results	Values
Cut-in speed (m/s)	0.5000
Rated speed (m/s)	1.0100
Cut-out speed (m/s)	1.4910
Normalized power	0.6548
Capacity factor (*CF*)	0.6355

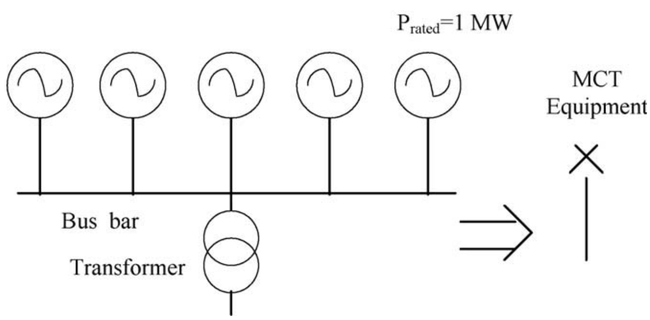


Fig. 8. A MCT group with five 1 MW MCTs.

of output states and average power output of the group are shown in Table 3. The calculated *CF* shown in Table 2 is used to calculate the turbine average power output. If the outage rate of each MCT is neglected, then the average power output of the MCT group would be 0.1589 MW higher which results in an overestimate of energy yield by 1391.964 MWh per year.

4.3. Reliability analyses results

The reliability indices of the four collection schemes described in Section 3.1 are calculated using the failure rate and repair time assumptions shown in Table 4.

Using the fault tree technique, the *NDE*s of the four collection schemes are calculated for cases with and without fuses which are installed between the MCT equipment and feeder. It can be seen from Table 5 that fuses with a small additional investment can be used to enhance the reliability of the energy collection system. In the following discussion, it is assumed that MCT equipment is always equipped with a fuse. As can be seen scheme c (U-ring design) has the best reliability performance. Compare to scheme a (radical design), its *NDE* is 2749 MWh/year lower. The results indicate that when the repair time is long, *NDE* would provide useful information in choosing an effective electricity collection scheme. However, it should be pointed out that the fault currents of ring structures will be higher than that of radial structure and could result in higher requirement in switchgear rating.

Table 4
Reliability data of the components involved.

Components	Failure rate (fr/yr)	Repair time (h)
Feeder	0.015	2160
$\text{Feeder}_{\text{MCT-MCT}}$	0.01	2160
$\text{Cable}_{\text{B,C,...,H}}$	0.01	2160
MV breaker	0.025	240
Platform breaker	0.025	72
MCT equipment	0.1	168

Table 5
*NDE*s of different electricity collection schemes.

Scheme	*NDE* (MWh/year) (without fuse)	*NDE* (MWh/year) (with fuse)
(a)	7437	4701
(b)	3824	3433
(c)	2343	1952
(d)	3447	3104

4.4. Cost analyses results

Connection structures with various cable sizes shown in Fig. 4 are studied. The lengths of submarine cables are 1.5 km between two adjacent MCT equipments and 5 km between MCF and platform (the 800 mm^2 cable). Information of XLPE cable impedances and shunt charging are available in [13]. The costs of equipment involved are listed in Table 6 [14]. Cost analyses are conducted based on the following assumptions: electric price is 0.15 $/kWh, O&M cost is 0.3 M$/year, discount rate is 5% and the economic life is 20 years. If the fixed loss is neglected, Table 7 shows the costs and *LCC* calculated. Variable loss cost is computed based on line losses obtained from power flow solutions of various electricity grid schemes. From Table 7, it can be seen that scheme c (U-ring design) has the lowest *LCC*. The U-ring design has the highest investment cost, but lowest variable loss and *NDE* costs. On the other hand, radical design (scheme a) has the lowest investment cost, but higher variable loss and *NDE* costs. Since *NDE* costs are higher than variable loss costs and contribute 11–

Table 6
Costs for equipment involved [14].

Equipment	Cost ($)
Breaker	135000
Fuse	10000
95 mm^2 conductor	152/m
150 mm^2 conductor	228/m
240 mm^2 conductor	250/m
300 mm^2 conductor	300/m
400 mm^2 conductor	381/m
630 mm^2 conductor	571/m
800 mm^2 conductor	600/m

Table 3
Probability of the turbine availability and average power output of the MCT group shown in Fig. 8.

State	No. of turbines in service	Total rated capacity (*C*, MW)	State probability P_s	Average power output (MW) ($C \times P_s \times CF$)
0	0	0	3.125E−07	0
1	1	1	2.96875E−05	1.88664E−05
2	2	2	0.001128125	0.001433847
3	3	3	0.021434375	0.040864636
4	4	4	0.203626563	0.517618723
5	5	5	0.773780938	2.45868893
Total			1.000000000	3.018625003

Table 7
Costs of different collection schemes.

Scheme	Investment costs (M$)	Variable loss costs		Not-delivered energy costs		O&M costs		Life-cycle costs *LCC* (M$)
		(M$/year)	PW (M$)	(M$/year)	PW (M$)	(M$/year)	PW (M$)	
(a)	17.99	0.71	8.848	0.71	8.848	0.3	3.739	39.425
(b)	19.78	0.33	4.113	0.52	6.480	0.3	3.739	34.112
(c)	24.87	0.068	0.847	0.29	3.614	0.3	3.739	33.070
(d)	22.45	0.200	2.492	0.47	5.857	0.3	3.739	34.538

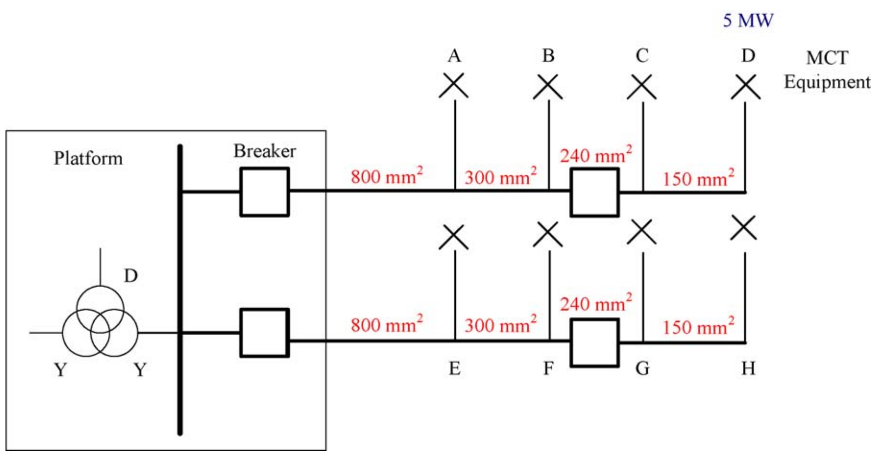


Fig. 9. Collection scheme (p).

22% (present worth) to *LCC*, it will affect the decision in adopting an electricity collection system for marine energy farm development.

Another collection scheme (scheme p) modified from scheme c by opening the loop and resizing the conductor is shown in Fig. 9. The *LCC* of this scheme is 31.727 M$, which is lower than those of other schemes. Scheme p has a better reliability performance when compared with that of scheme a. This scheme also has a lower investment cost than that of scheme c. Therefore, scheme p is capable of keeping a good balance between cable cost and system reliability. Using the techniques presented, one could pursue better design with lower *LCC* for marine energy collection.

5. Conclusion

A brief review of offshore wind farm design is given and an analytical procedure for cost analyses of electricity collection systems with emphasis on system reliability of a marine current farm is presented. A new methodology is proposed to determine the speed specifications of MCT. Analytical results show that the probability density function of ocean current speeds used in this study is a normal distribution, and based on this distribution *TPI* formulation is derived and used to determine turbine speed specifications in order to achieve higher energy output and capacity factor. The importance of unavailability cost is highlighted in the test result. It shows that, among the collection schemes investigated, U-ring design has the best reliability performance and lower *LCC*. However, numerical result also shows that a simple modified scheme could also provide an effective solution for marine energy collection.

Appendix A

Normal distribution is expressed as:

$$f(v) = \frac{1}{\sqrt{2\pi}\sigma}\exp\left[-\frac{(v-\mu)^2}{2\sigma^2}\right] \tag{A.1}$$

The capacity factor, *CF*

$$\begin{aligned} &= \frac{P_{e,ave}}{P_{eR}} = \frac{\int_0^\infty P_e(v)\,f(v)\,dv}{P_{eR}} \\ &= \frac{\int_{v_C}^{v_R}(1/2)\rho AC_p\eta v^3\,f(v)\,dv + \int_{v_R}^{v_F}(1/2)\rho AC_p\eta v_R^3\,f(v)\,dv}{(1/2)\rho AC_p\eta v_R^3} \\ &= \frac{1}{v_R^3}\int_{v_C}^{v_R} v^3\,f(v)\,dv + \int_{v_R}^{v_F} f(v)\,dv = CF_1 + CF_2 \end{aligned} \tag{A.2}$$

$$CF_1 = \frac{1}{v_R^3}\int_{v_C}^{v_R} v^3 \frac{1}{\sqrt{2\pi}\sigma}\exp\left(-\frac{(v-\mu)^2}{2\sigma^2}\right)dv \tag{A.3}$$

Let $x = (v-\mu)/\sqrt{2}\sigma$, and then $dx = dv/\sqrt{2}\sigma$

$$CF_1 = \frac{1}{v_R^3\sqrt{\pi}}\int_a^b \left(\sqrt{2}\sigma x + \mu\right)^3 \exp(-x^2)\,dx \tag{A.4}$$

where $a = (v_C-\mu)/\sqrt{2}\sigma$, $b = (v_R-\mu)/\sqrt{2}\sigma$

$$\begin{aligned} CF_1 = {} & \frac{2\sqrt{2}\sigma^3}{v_R^3\sqrt{\pi}}\int_a^b x^3\exp(-x^2)\,dx + \frac{6\sigma^2\mu}{v_R^3\sqrt{\pi}}\int_a^b x^2\exp(-x^2)\,dx \\ & + \frac{3\sqrt{2}\sigma\mu^2}{v_R^3\sqrt{\pi}}\int_a^b x\exp(-x^2)\,dx + \frac{\mu^3}{v_R^3\sqrt{\pi}}\int_a^b \exp(-x^2)\,dx \end{aligned} \tag{A.5}$$

According to Steen's deduction for integration $\int_0^b \exp(-x^2) f(x)\,dx$ by using Gaussian quadratures in 1969 [15], *CF* can be calculated by the following equation:

$$\begin{aligned} CF_1 = {} & \frac{2\sqrt{2}\sigma^3}{v_R^3\sqrt{\pi}}[I3(b) - I3(a)] + \frac{6\sigma^2\mu}{v_R^3\sqrt{\pi}}[I2(b) - I2(a)] \\ & + \frac{3\sqrt{2}\sigma\mu^2}{v_R^3\sqrt{\pi}}[I1(b) - I1(a)] + \frac{\mu^3}{v_R^3\sqrt{\pi}}[I0(b) - I0(a)] \end{aligned} \tag{A.6}$$

where

$$I0(\alpha) = \int_0^\alpha \exp(x^2)\,dx = \frac{1}{2}\sqrt{\pi} \times erf(\alpha) \tag{A.7}$$

$$I1(\alpha) = \int_0^\alpha x\exp(x^2)\,dx = \frac{1}{2}[1 - \exp(-\alpha^2)] \tag{A.8}$$

$$I2(\alpha) = \int_0^\alpha x^2\exp(x^2)\,dx = \frac{1}{4}\sqrt{\pi} \times erf(\alpha) - \frac{1}{2}\alpha \times \exp(-\alpha^2) \tag{A.9}$$

$$I3(\alpha) = \int_0^\alpha x^3\,exp(x^2)\,dx = \frac{1}{2}[1 - exp(-\alpha^2) - \alpha^2 \times exp(-\alpha^2)] \tag{A.10}$$

$erf(\boldsymbol{\alpha})$ is the error function, it is defined as the following equation:

$$erf(\alpha) = \frac{2}{\sqrt{\pi}}\int_0^\alpha \exp(-t^2)\,dt \tag{A.11}$$

In a similar way:

$$CF_2 = \int_{v_R}^{v_F} \frac{1}{\sqrt{2\pi}\sigma}\,exp\left(-\frac{(v-\mu)^2}{2\sigma^2}\right)dv \tag{A.12}$$

Let $x = (v-\mu)/\sqrt{2}\sigma$, and then $dx = dv/\sqrt{2}\sigma$

$$CF_2 = \frac{1}{\sqrt{2\pi}\sigma}\cdot\sqrt{2}\sigma\int_b^c e(-x^2)\,dx \tag{A.13}$$

where b is defined as before, $c = (v_F-\mu)/\sqrt{2}\sigma$

$$CF_2 = \frac{1}{\sqrt{\pi}}(I0(c) - I0(b)) \tag{A.14}$$

From the above deduction, it indicates that CF is a function of a, b and c. Therefore, CF is also a function of cut-in speed v_C, rated speed v_R and cut-out speed v_F, and can be described by a closed form function.

References

[1] Boyle G. Renewable energy—power for a sustainable future, 2nd ed., United Kingdom: Oxford University Press; 2004.

[2] Jangamshetti SH, Rau VG. Normalized power curves as a tool for identification of optimum wind turbine generator parameters. IEEE Trans Energy Convers 2001;16(3):283–8.

[3] Bahaj AS, Myers L. Analytical estimates of the energy yield potential from the Alderney Race (Channel Islands) using marine current energy converters. Renew Energy 2004;29:1931–45.

[4] Larsen JHM, Soerensen HC, Christiansen E, Naef S, Vølund P. Experience from Middelgrunden 40 MW offshore wind farm. In: Copenhagen offshore wind conference; 2005.

[5] Sannino A, Breder H, Nielsen EK. Reliability of collection grids for large offshore wind parks. In: Proceedings of 9th international conference on probabilistic methods applied to power systems; 2006.

[6] Quinonez-Varela G, Ault GW, Anaya-Lara O, McDonald JR. Electrical collector system options for large offshore wind farms. IET Renew Power Gener 2007;1(2):107–14.

[7] Conover WJ. A Kolmogorov goodness-of-fit test for discontinuous distributions. J Am Stat Assoc 1972;67(339):591–6.

[8] Bedard R, Previsic M, Siddiqui O, Hagerman G, Robinson M. Survey and characterization tidal in stream energy conversion (TISEC) devices. EPRI-TP-004 NA; 2005.

[9] Sen Z. Statistical investigation of wind energy reliability and its application. Renew Energy 1997;10(1):71–9.

[10] Manwell JF, McGowan JG, Rogers AL. Wind energy explained—theory, design and application. New York: Wiley; 2002.

[11] Billinton R, Allan RN. Reliability evaluation of power systems. New York and London: Plenum Press; 1984.

[12] Walling RA, Ruddy T. Economic optimization of offshore windfarm substations and collection systems. In: Proceedings of fifth international workshop on large-scale integration of wind power and transmission networks for offshore wind farms; 2005.

[13] http://search.abb.com/library/Download.aspx?DocumentID=2GM5007%20GB%200501&LanguageCode=en&DocumentPartID=&Action=Launch&IncludeExternalPublicLimited=True.

[14] Green J, Bowen A, Fingersh LJ, Wan Y. Electrical collection and transmission systems for offshore wind power. In: 2007 offshore technology conference; 2007.

[15] Steen NM, Byrne GD, Celbard EM. Gaussian quadratures for the integrals $\int_0^\infty \exp(-x^2)f(x)\,dx$ and $\int_0^b \exp(-x^2)f(x)\,dx$. Math Comput 1969;23(107):661–71.